Tryptophan and tryptophan-like substances in cloud water: Occurrence and photochemical fate

Angelica Bianco, Monica Passananti, Laurent Deguillaume, Gilles Mailhot, Marcello Brigante

Tryptophan and tryptophan-like substances in cloud water: Occurrence and photochemical fate

Angelica Bianco [a, b], Monica Passananti [a, b], Laurent Deguillaume [c, d], Gilles Mailhot [a, b], Marcello Brigante [a, b, *]

[a] Université Clermont Auvergne, Université Blaise Pascal, Institut de Chimie de Clermont-Ferrand, BP 10448, F-63000 Clermont-Ferrand, France
[b] CNRS, UMR 6296, ICCF, F-63171 Aubiere, France
[c] Université Clermont Auvergne, Université Blaise Pascal, OPGC, Laboratoire de Météorologie Physique, BP 10448, F-63000 Clermont-Ferrand, France
[d] CNRS, UMR 6016, LaMP/OPGC, BP80026, F-63177 Aubière, France

HIGHLIGHTS

- Tryptophan and tryptophan-like substances were quantified in cloud water sampled at the puy de Dôme station.
- The fate of tryptophan was investigated in the cloud aqueous phase under sun-simulated conditions.
- The hydroxyl radical-mediated transformation of tryptophan in cloud water can be considered to be a source of carboxylic compounds.

GRAPHICAL ABSTRACT

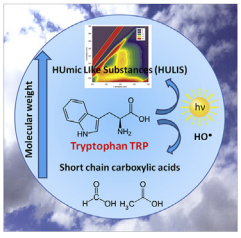

ARTICLE INFO

Article history:
Received 9 March 2016
Received in revised form
22 April 2016
Accepted 24 April 2016

Keywords:
Cloud water
Photochemistry
Organic matter
Amino acids

ABSTRACT

This work investigates the occurrence and photochemical behaviour of tryptophan (TRP) in the cloud aqueous phase. The concentrations of tryptophan, TRYptophan LIke Substances (TRYLIS) and HUmic LIke Substances (HULIS) in real cloud water, collected between October 2013 and November 2014 at the top of the puy de Dôme station, were determined using the Excitation-Emission-Matrix (EEM) technique. The amount of free and complexed tryptophan (TRP) up to 10^{-7} M in cloud aqueous phase was quantified by HPLC-UV-fluorescence analysis, and its photoreactivity under sun-simulated conditions was investigated in synthetic water samples mimicking cloud aqueous phase compositions (oceanic and continental origins). TRP undergoes direct photolysis, and its degradation is enhanced in the presence of naturally occurring species able to photo-generate hydroxyl radicals (HO•). The polychromatic quantum yield of TRP ($\varphi^{TRP}_{290-340nm}$) is estimated to be 8.37×10^{-4} between 290 and 340 nm, corresponding to the degradation rate (R^{d}_{TRP}) of 1.29×10^{-11} M s^{-1} under our irradiation conditions. The degradation is accelerated up to 3.65×10^{-10} and 8.26×10^{-10} M s^{-1} in synthetic oceanic and continental cloud water samples doped with 100 μM hydrogen peroxide, respectively.

Hydroxyl radical-mediated transformation leads to the generation of different functionalized and oxidized products, as well as small carboxylic acids, such as formate and acetate. Moreover, fluorescent signals of irradiated solutions indicate the formation of HULIS.

1. Introduction

In the atmosphere, Primary Biological Aerosols (PBA) are

* Corresponding author. Université Clermont Auvergne, Université Blaise Pascal, Institut de Chimie de Clermont-Ferrand, BP 10448, F-63000 Clermont-Ferrand, France.
E-mail address: marcello.brigante@univ-bpclermont.fr (M. Brigante).

ubiquitous and are comprised of either biological particles, including dead or live cells, or cell fragments (Deguillaume et al., 2008; Després et al., 2012; Zhu et al., 2015). They are able to nucleate cloud droplets and ice particles *via* physical processes (Möhler et al., 2007; Morris et al., 2014; Spracklen and Heald, 2014). PBA are mainly made up of organic substances and contribute to aerosol masses (organic carbon fraction, OC), and the organic fraction resulting from PBA components is made of biological compounds such as proteins and/or amino acids. These amino compounds were found to account for a significant fraction of fine particulate matter (Ge et al., 2011). For example, Zhang et al. (2002) showed that amino acids can represent between 1.6 and 14% of the $PM_{2.5}$ mass at Davis in California. Several sources can be responsible for the atmospheric amino acid content; over a continental area, the biological compounds are produced by plants, pollen, algae, fungi and bacteria spores (Mace et al., 2003a; Milne and Zika, 1993; Scheller, 2001; Zhang and Anastasio, 2003). Human activities can also lead to the input of amino acids into the atmosphere. Zhang and Anastasio (2003) identified livestock farming as the most important source of amino acids over the Californian region. These compounds are also present on anthropogenic coarse particles; soil and desert dust are also probably important sources of amino acids (Mace et al., 2003b). Moreover, marine emissions can also influence the atmospheric concentrations of amino acids (Matsumoto and Uematsu, 2005), as confirmed by Wedyan and Preston (2008) over the southern Atlantic Ocean. Finally, amino acids can be ejected into the atmosphere by volcanoes (Scalabrin et al., 2012) or by biomass burning (Chan et al., 2005; Mace et al., 2003a).

Amino acids can influence the microstructure of aerosol particles and consequently their water uptake, thus modifying cloud formation (Hock et al., 2008; McFiggans et al., 2006; Schwier et al., 2013). They can also act as ice-forming nuclei due to their hygroscopicity (Wedyan and Preston, 2008), leading to the formation of new particles in the atmosphere (De Haan et al., 2009).

These compounds belong to the Water-Soluble Organic Compounds (WSOC) and consequently dissolve into the atmospheric aqueous phase. Several studies have reported concentrations of amino acids in the condensed phase of aerosols (Barbaro et al., 2015; Mandalakis et al., 2011; Mochizuki et al., 2015; Zhang and Anastasio, 2003) as well as in rainwater and fog (Zhang and Anastasio, 2001). For example, the total amino acids have been evaluated to account for 13% of the Dissolved Organic Carbon (DOC) in fog waters and approximately 10% of the WSOC in $PM_{2.5}$ (Zhang and Anastasio, 2003). Amino acids should also be present in cloud water and could contribute to the dissolved organic content of cloud water that is currently still not well characterized (Herckes et al., 2013; Herrmann et al., 2015).

In atmospheric water and aerosols, amino acids have been classified into the following different categories: DFAA (Dissolved Free Amino Acids), which indicates the free amino acids, and DCAA (Dissolved Combined Amino Acids), which indicates peptides, proteins and free amino acids that are also constituents of humic and fulvic acids (Kuznetsova et al., 2005). Another classification distinguishes between FAC (Free Amino Compounds), which are comprised of amino acids and alkyl amines, and CAC (Combined Amino Compounds) if they are free or combined in proteins, peptides or HULIS substances (Zhang and Anastasio, 2003).

Amino acids, and more particularly TRP, present in atmospheric water can directly absorb sun radiation or react with oxidants leading to the formation of inorganic and organic products (Creed, 1984; McGregor and Anastasio, 2001; Milne and Zika, 1993; Suzuki et al., 1985; Zhang and Anastasio, 2003). Their reactivity can therefore modify the chemical composition of dissolved organic matter changing the chemical properties of water droplets and thus of aerosol particles.

Currently, scarce data are present in the literature on the occurrence and fate of amino acids or amino compounds in atmospheric water. To our knowledge, only Muller et al. (2008) have previously reported the presence of TRYptophan LIke Substances (TRYLIS) in rainwater. In our work, we quantified the TRP concentration and detected the presence of TRYLIS and HUmic-LIke-Substances (HULIS) in cloud water samples collected at the puy de Dôme mountain station (France). To assess the possible impact on the aqueous organic chemical composition, TRP solutions are irradiated under sun-simulated conditions and transformation products are characterized. Oxidation processes occur and lead to the formation of carboxylic acids, as well as HULIS, which are followed during our experiments.

2. Materials and methods

2.1. Sampling method

A total of 23 cloud samples were collected during two field campaigns in October and November 2013 and in March and April 2014 at the top of puy de Dôme mountain (1465 m a.s.l.) in France that belongs to the GAW (Global Atmosphere Watch) stations network. Cloud samples are spread among the following three classes: marine, highly marine and continental following the statistical analysis from Deguillaume et al. (2014).

The cloud droplet sampling was carried out by a one stage cloud droplet impactor. The sampling times ranged from 120 to 180 min depending on the Liquid Water Content (LWC), which was in the range of 0.1–0.2 g cm^{-3}.

2.2. Chemical analysis

In order to characterize the main physicochemical properties of the sampled solution, the following physico-chemical measurements are performed immediately after cloud sampling and filtration: conductivity, redox potential, pH, UV–visible spectrum, and Excitation Emission Matrix (EEM) are carried out in less than one hour, while ion chromatography, quantification of the nitrite concentration and determination of the Total Organic Carbon (TOC) were performed on frozen samples. Analyses on frozen samples (kept at 255 K) are carried out in less than 48 h after sampling. The results of the physico-chemical analysis are reported in Bianco et al. (2015).

2.3. Irradiation experiments

One hundred millilitre aliquots of TRP solutions are irradiated in a photoreactor placed in a cylindrical stainless steel container. Six fluorescent lamps (Philips TL D15W/05), whose emission spectrum ranges from 290 to 500 nm, are separately placed along three different axes, while the photoreactor, a Pyrex tube with a 2.6 cm internal diameter, is placed in the centre of the setup. All of the experiments are carried out at 278 ± 2 K. An aliquot of the solution (3 mL) is withdrawn from the reactor and used for analysis at fixed times. In Fig. 1, the emission spectrum of the lamp recorded using fibre optics coupled with a CCD spectrophotometer (Ocean Optics USD 2000+UV–VIS) is reported. The energy has been normalized to the actinometry results using paranitroanisole (PNA)/pyridine actinometer (Dulin and Mill, 1982). Over the UV region (wavelength range 290–400 nm), a total flux of 15.8 W m^{-2} is measured. The adopted intensity was close to the intensity measured between 290 and 400 nm at the top of puy de Dôme mountain during a late-autumn cloudy day at 11:00a.m. (see Fig. 1). Moreover, the absorption spectrum of TRP in water at a pH of 6.0 is reported in Fig. 1, showing an overlap with the emission spectrum of the irradiation

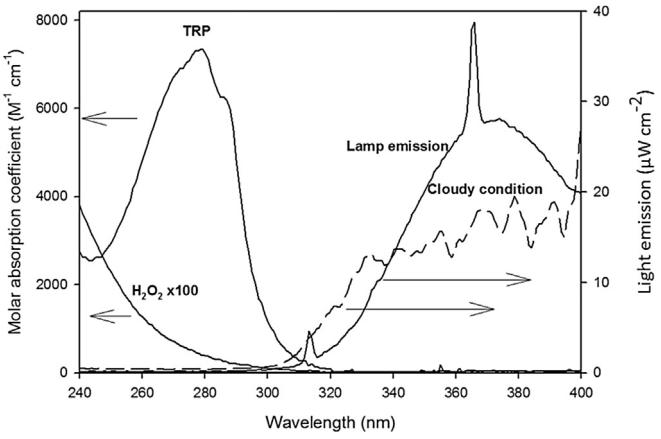

Fig. 1. Left axis: absorption spectra of TRP and H_2O_2 (×100) aqueous solutions. Right axis: emission spectrum of the fluorescent lamps reaching solutions over the range of 290–400 nm (total flux intensity of 2039 μW cm^{-2}) compared with the sun emission spectrum (dashed line) for a cloudy day (1580 μW cm^{-2}) in October 2013.

setup.

TRP (10 μM) is irradiated in pure Milli-Q water and in synthetic water samples mimicking the chemical composition of cloud water doped with H_2O_2 (from 100 μM to 10 mM). Two different synthetic water samples are prepared; the first one is representative of marine cloud water and the second is a solution of continental cloud water (see Table SM1 for the chemical composition).

2.4. Fluorescence characterization of samples

Fluorescence chromophores are identified in real cloud water samples on the basis of previously reported data (Coble, 1996; Mayer et al., 1999) using an Excitation Emission Matrix (EEM).

EEM are recorded with a Varian Cary Eclipse Fluorescence Spectrophotometer with 5 nm intervals for excitation wavelengths from 200 to 500 nm and emission from 220 to 600 nm with scan rate of 600 nm min^{-1} and bandpass of 10 nm for both excitation and emission. Standard solutions of TRP (between 1×10^{-9} and 5×10^{-7} M) were used to calibrate the fluorescence signal. The following two signals are considered: the first one at λ_{ex} 225 nm and λ_{em} 330 nm and the second one at λ_{ex} 275 nm and λ_{em} 340 nm. Many other compounds could present fluorescence emission at λ_{ex} 225 nm; for this reason, the second signal at $\lambda_{ex}/\lambda_{em}$ 275/330 nm is considered for calibration. The limit of detection of this method is estimated to be 5×10^{-10} M according to the signal/noise ratio of the instrument.

2.5. Chromatographic analysis and kinetics

The TRP concentration was determined in cloud water samples and in synthetic solutions prepared with Milli-Q water. Quantification was performed with a Waters Acquity Ultra Performance LC equipped with Water Acquity Photo Diode Array detector and fluorescence detector. Compound separation was performed using a Waters Acquity UPLC C18 column (100 mm × 2.1 mm × 1.7 μm) and isocratic elution with 90% acetate buffer (2.5 mM) and 10% methanol. The eluent flow rate was 0.3 mL min^{-1}, and the retention time of TRP is 2.7 min. Fluorescence detection is performed with $\lambda_{ex} = 225$ nm and $\lambda_{em} = 340$ nm.

The initial rates of TRP degradation were determined by fitting the experimental data with the pseudo-first order decay equation of the form $[TRP]_t = [TRP]_0 \exp(-k^d_{TRP} \times t)$, where $[TRP]_0$ and $[TRP]_t$ are the concentrations of TRP at the initial time and time t, respectively, and k^d_{TRP} is the pseudo-first order decay constant. The TRP degradation rate (R^d_{TRP}, M s^{-1}) could then be obtained from $k^d_{TRP} \times [TRP]_0$.

The polychromatic degradation quantum yield ($\phi^{TRP}_{290-350nm}$) is also calculated. $\phi^{TRP}_{290-350nm}$ is defined as the ratio between the number of molecules transformed and the number of photons absorbed in the same period of time (Eq. (1)):

$$\phi^{TRP}_{290-350nm} = \frac{R^d_{TRP}}{I_a} \quad (1)$$

where R^d_{TRP} is the TRP degradation rate (M s^{-1}) and I_a is the absorbed photon flux per unit of surface and unit of time. The latter was calculated from Eq. (2):

$$I_a = \int_{\lambda} I_0(\lambda)\,(1 - 10^{-\varepsilon(\lambda)\mathrm{d}[\mathrm{TRP}]_0}) \quad (2)$$

where I_0 is the incident photon flux, ε the molar absorption coefficient of TRP, d the optical path length inside the cell and $[TRP]_0$ is the initial TRP concentration.

2.6. Transformation product identification

With the objective of detecting the photoproducts, more concentrated TRP solutions (200 μM) are irradiated in the presence and absence of hydrogen peroxide (1 mM) and analysed by LC-MS with ESI (Electro Spray Ionization) in the positive mode, followed by detection by tandem mass spectrometry using a qTOF (quadrupole time of flight) detector. A resolution of 5000 was used for the TOF-MS analyses.

Ion Chromatography (IC) analyses are performed using a DIONEX DX-320 equipped with an IonPac AG18 (guard column, 2 × 50 mm) and an IonPac AS18 (analytical column 2 × 250 mm). Elution is performed with a gradient of 10 mM potassium hydroxide to 20 mM in 30 min and with a prior stabilization for 5 min at 10 mM. The injection loop volume is fixed to 750 μL. Under these conditions, the retention times of acetate and formate are of 6.5 and 7.3 min, respectively.

3. Results and discussion

3.1. Fluorescence characterization of cloud aqueous phase samples

In Fig. 2, the EEM spectra of cloud aqueous phase samples 4 and 9 (see Table 1) are reported for illustration. In both spectra (Fig. 2, graphics 4-A and 9-A) obtained using an intensity range scale from 0 to 50 or 60, different peaks can be observed. The first peak is centred at $\lambda_{ex}/\lambda_{em}$ 225/340 nm with a high intensity signal, and the other two peaks can be detected using a lower intensity scale (from 0 to 20) at $\lambda_{ex}/\lambda_{em}$ 275/330 nm and $\lambda_{ex}/\lambda_{em}$ 310/410 nm (see Fig. 2, graphics 4-B and 9-B). The TRP signal in pure water is reported in Figure SM1, where two EEM peaks are present at $\lambda_{ex}/\lambda_{em}$ 225/360 nm and $\lambda_{ex}/\lambda_{em}$ 275/360 nm. Tryptophan-like substances are detected in our samples from the signal intensity at $\lambda_{ex} = 225$ nm and $\lambda_{em} = 330$ nm (see Table 1). The fluorescence signal is normalized for the Raman intensity peak at 350 nm, and the concentration is calculated with the calibration reported in Figure SM2. TRYLIS signals in the cloud aqueous phase present a blue-shift emission as reported when amino acids are combined. Fluorescence in the natural environment may be different to that observed in the laboratory under controlled conditions using pure amino acid solutions. Protein fluorescence resembles that of amino acids, as observed by Mayer et al. (1999). Most of the intrinsic

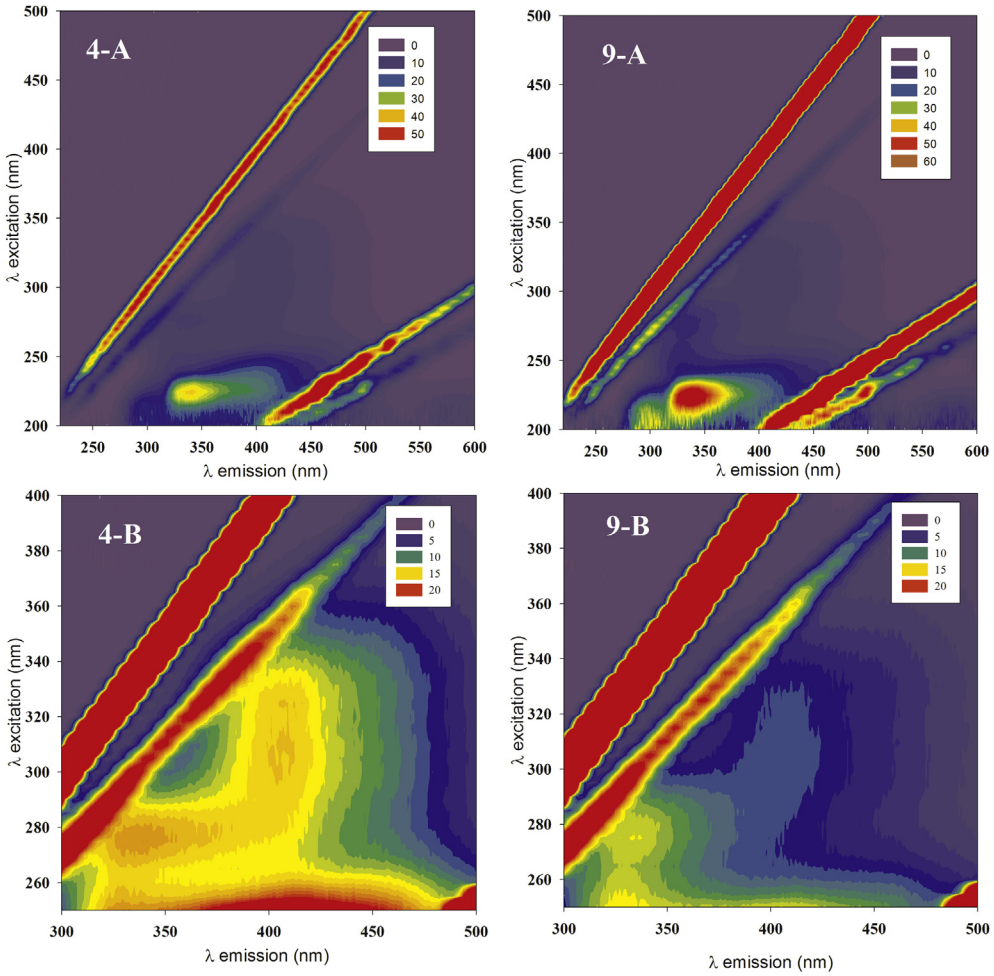

Fig. 2. EEM (as contour plot) of samples 4 and 9. For 4-**A** and 9-**A**, excitation ranges from 200 to 500 nm and emission from 220 to 600 nm. The intensity is scaled from 0 to 50 or 60. For 4-**B** and 9-**B**, excitation ranges from 250 to 400 nm and emission from 300 to 500 nm. Intensity is scaled from 0 to 20. The linear features (in red) are Rayleigh scattering in water. (For interpretation of the references to colour in this figure legend, the reader is referred to the web version of this article).

fluorescence emission is due to the excitation of TRP residues (quantum yield of fluorescence of 0.20), with some emission due to tyrosine (TYR, with a fluorescence quantum yield of 0.14) or phenylalanine (PHE, with a fluorescence quantum yield of 0.04). TRP fluorescence emission is dominant over the weaker signals of TYR and PHE. The signal of TRP is influenced by the proximity of other amino acid residues; the signal could be shifted or quenched, especially by aspartate (ASP) or glutamate (GLU) residues (Vivian and Callis, 2001). Many authors found a blue shift to shorter emission wavelengths due to differences in the behaviour of amino acids in the different microenvironments present within proteins. Determann et al. (1998) detect TRP and TRYLIS in seawater with $\lambda_{ex}/\lambda_{em}$ 230/350 nm, and Hudson and co-workers (Hudson et al., 2007) show that there are two signals with the first one at λ_{ex} 225–237 nm and λ_{em} 340–381 nm and the less intense second signal at $\lambda_{ex}/\lambda_{em}$ 275/310 nm.

Many compounds could present a fluorescent signal with excitation at λ_{ex} 225 nm, and the concentration could be overestimated. For this reason, TRP is detected and quantified in EEM from the signal intensity at $\lambda_{ex}/\lambda_{em}$ 275/330 nm. The concentration is calculated with the calibration reported in Figure SM2. The average concentration of TRP is $1.7 \pm 1.1 \times 10^{-7}$ M. The EEM method is not able to distinguish between free and combined TRP, so the reported concentration values correspond to the total concentration of TRP. We quantified free TRP by UPLC-FLR, and the data are shown in Table 1. The limit of detection (LOD), based on the signal/noise ratio of the instrument, allows the determination of concentrations up to 5×10^{-9} M. TRP is not detected in all of the samples; however, when TRP is detected, the average concentration is $5.8 \pm 6.2 \times 10^{-8}$ M. Considering that the concentration of the sum of free and combined TRP is estimated to be approximately 1.7×10^{-7} M, free TRP represents less than 37% of the total TRP in cloud water.

3.2. TRP photoreactivity

Different irradiation experiments using 10 μM TRP solutions were performed in Milli-Q and synthetic cloud water doped with H_2O_2 (used as photochemical source of hydroxyl radicals) in order to investigate the photoreactivity and fate of TRP. Under direct photolysis, TRP undergoes slow degradation, with up to 5% disappearance after 4 h of irradiation, and the polychromatic quantum yield between 290 and 350 nm ($\phi^{TRP}_{290-350nm}$) is estimated to be 8.37×10^{-4}.

In the presence of different H_2O_2 concentrations (100 μM, 1 mM and 10 mM), TRP degradation rates increase from 1.29×10^{-11} M s^{-1} in pure water to 4.32×10^{-10} M s^{-1} in the presence of H_2O_2 (10 mM) corresponding to a hydroxyl radical formation rate of $R^{f}_{HO^{\bullet}} = 2.78 \pm 0.01 \times 10^{-8}$ M s^{-1} (see Figure SM2). Under our experimental conditions, a fraction of the

Table 1
TRP-like concentrations and emission intensities of HULIS taken normalizing the Raman signal (350 nm) at 500 A.U.

Sampling			Tryptophan-like signal (M)*	Tryptophan *UPLC-FLR*	HULIS signal (A.U.)
Period (dd/mm/yyyy)	Sampling time	Sample number			λ_{ex} = 340 nm λ_{em} = 420 nm
14/10/2013	4 p.m.–6 p.m.	1	1.1×10^{-7}	$2.4 \pm 0.7 \times 10^{-8}$	29.8
14/10/2013	6 p.m.–9 p.m.	2	6.1×10^{-8}	ND	12.3
14/10/2013	9 p.m.–12 p.m.	3	1.4×10^{-7}	ND	20.7
29/10/2013	5 a.m.–8 a.m.	4	3.6×10^{-7}	$1.7 \pm 0.2 \times 10^{-7}$	52.8
29/10/2013	8 a.m.–12 a.m.	5	1.1×10^{-7}	ND	15.9
05/11/2013	2 p.m.–4 p.m.	6	8.4×10^{-8}	ND	13.1
05/11/2013	4 p.m.–7 p.m.	7	2.6×10^{-7}	ND	25.8
05/11/2013	7 p.m.–9 p.m.	8	1.6×10^{-8}	$9.4 \pm 0.5 \times 10^{-8}$	2.8
05/11/2013	9 p.m.–12 p.m.	9	1.6×10^{-7}	ND	15.3
06/11/2013	7 a.m.–10 a.m.	10	2.5×10^{-7}	ND	20.6
06/11/2013	10 a.m.–12 a.m.	11	1.8×10^{-7}	ND	21.3
22/03/2014	7 a.m.–11 a.m.	12	1.1×10^{-7}	$2.7 \pm 0.5 \times 10^{-8}$	15.5
22/03/2014	11 a.m.–2 p.m.	13	1.0×10^{-7}	ND	14.0
25/03/2014	11 a.m.–1 p.m.	14	2.8×10^{-7}	ND	22.2
25/03/2014	1 p.m.–3 p.m.	15	3.9×10^{-7}	$1.6 \pm 0.5 \times 10^{-8}$	25.5
25/03/2014	7 p.m.–9 p.m.	16	4.4×10^{-7}	$1.5 \pm 0.5 \times 10^{-8}$	22.2
26/03/2014	8 a.m.–9 a.m.	17	1.1×10^{-7}	ND	27.9
26/03/2014	9 a.m.–11 a.m.	18	1.2×10^{-7}	ND	15.3
01/04/2014	8 p.m.–10 p.m.	19	1.1×10^{-7}	ND	7.7
01/04/2014	10 p.m.–12 p.m.	20	1.1×10^{-7}	ND	10.0
01/04/2014	1 p.m.–4 a.m.	21	1.2×10^{-7}	ND	9.6
01/04/2014	4 a.m.–7 a.m.	22	9.3×10^{-8}	ND	10.8
01/04/2014	7 a.m.–10 a.m.	23	1.3×10^{-7}	ND	11.7

ND: quantification not determined because the signal was lower than the detection limit of 1 nM.
* The value was estimated considering the fluorescence signal of pure TRP solution.

photogenerated hydroxyl radicals also reacts with the source (H_2O_2). It is then possible to quantify the fraction of hydroxyl radicals reacting with TRP for each experimental condition considering the initial concentration of H_2O_2 in the solution and the related second order rate constants with HO• ($k_{HO^\bullet,H_2O_2} = 2.7 \times 10^7\ M^{-1}\ s^{-1}$) (Buxton et al., 1998). TRP degradation can be quantitatively attributed to the hydroxyl radical as shown in Fig. 3, where a linear correlation between R^d_{TRP} and the hydroxyl radical formed (making the radicals available to react with TRP) is found.

In order to better understand the behaviour of TRP in cloud water, synthetic water samples are prepared on the basis of the concentrations of anions found in real cloud water (Bianco et al., 2015) (see Table SM1). To maintain the same ratio between TRP and the inorganic compounds, the average concentration of anions is multiplied by a factor 10.

Fig. 4 reports the kinetic profiles for 10 μM TRP in the presence of Milli-Q and synthetic cloud water samples doped with 100 μM of H_2O_2. In the oceanic and continental synthetic water samples, TRP degradation is increased by approximately 3.5 and 10 times, respectively, compared to the value with an initial concentration of 100 μM H_2O_2 in pure water. This trend can be explained by considering the presence of nitrates (NO_3^-) and nitrites (NO_2^-) that provide an additional source of HO• (Bianco et al., 2015).

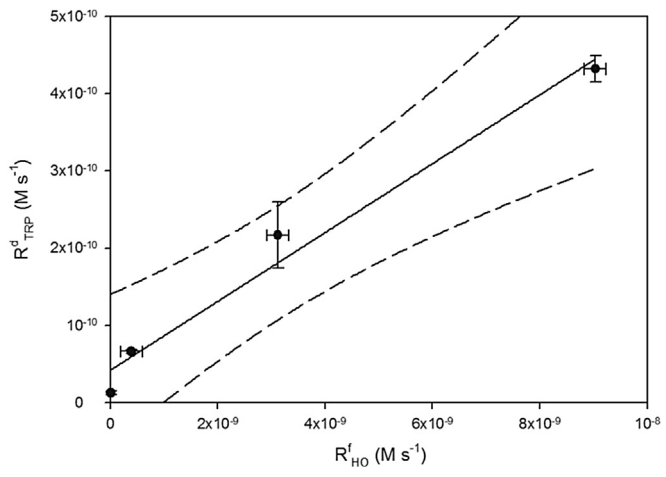

Fig. 3. Correlation between the initial transformation rate of TRP (R^d_{TRP}, M s^{-1}) and the formation rate of hydroxyl radicals (R^f_{HO}•, M s^{-1}). The experiment was performed using an initial TRP concentration of 10 μM and varying the H_2O_2 concentration between 0 and 10 mM. The error bars represent the 3σ based on the linear fit of experimental data, and dashed lines denote the 95% confidence of the linear fit.

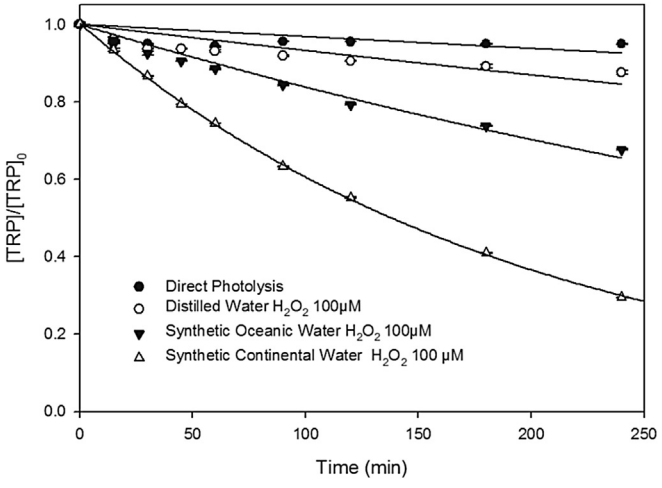

Fig. 4. Irradiation time-dependent concentration of TRP (10 μM) under polychromatic irradiation in the presence of H_2O_2 (100 μM) in distilled water or in synthetic cloud water mimicking the continental or oceanic origin scenario. The pH was set to 4.5 for the continental and 5.6 for the marine synthetic water samples, and the temperature was 288 ± 3 K.

3.3. Transformation mechanism

TRP (10 μM) is irradiated in the presence of 1 and 10 mM hydrogen peroxide. Irradiated solutions are analysed by Ion Chromatography for quantification of the carboxylic acid concentrations and by HPLC-fluorescence analysis for estimation of the fate of TRP (Fig. 5). After 4 h of irradiation and with 1 mM H_2O_2, TRP disappearance leads to the formation of 0.74 μM acetate and 0.37 μM formate. In the presence of 10 mM hydrogen peroxide, a complete disappearance of TRP is reported, leading to the formation of 2.0 μM acetate and formate (Fig. 5). After 4 h of irradiation, acetate and formate concentrations represent less than 10% of the initial carbon concentration (mgC L^{-1}), and thus the carbon gap indicates the formation of other organic compounds. A plausible interpretation of the photochemical and HO•-induced transformation of TRP is reported in Fig. 6. TRP can undergo the following two different transformation pathways: hydroxyl radical addition (*i* and *ii*) and hydrogen abstraction (*iii*). Hydroxyl radical addition (*i*) can lead to the formation of mono- and di-hydroxylate derivatives detected by LC-MS at $[M+H]^+ = 221$ m/z and at $[M+H]^+ = 237$ m/z, respectively. The hydroxylation of tryptophan occurs in different positions of the molecule yielding several possible hydroxytryptophan isomers. Unfortunately, in this case mass spectrometry does not allow understanding of which position on the aromatic ring the hydroxyl functional group is located (Domingues et al., 2003). The addition of HO• (*ii*) could take place on the pyrrolic ring, and the oxidative opening of the five-membered ring can lead to *N*-formylkynurenine ($[M+H]^+ = 237$ m/z). The oxidative opening of the pyrrolic ring has been previously observed for other indole derivatives (Turjanski et al., 1998). Formation of *N*-formylkynurenine from TRP oxidation has been previously reported (Domingues et al., 2003). The reactivity of molecular oxygen, after HO• addition, can occur as previously suggested for several amino acids (Milne and Zika, 1993) and could lead to the formation of 2-hydroxyindoline-3-carbaldehyde ($[M+H]^+ = 164$ m/z). This product could undergo further oxidation to form 2-oxoindoline-3-carbaldehyde and 2-oxoindoline-3-carboxylic acid detected by MS at $[M+H]^+ = 162$ m/z and $[M+H]^+ = 178$ m/z, respectively (Hinman and Lang, 1965).

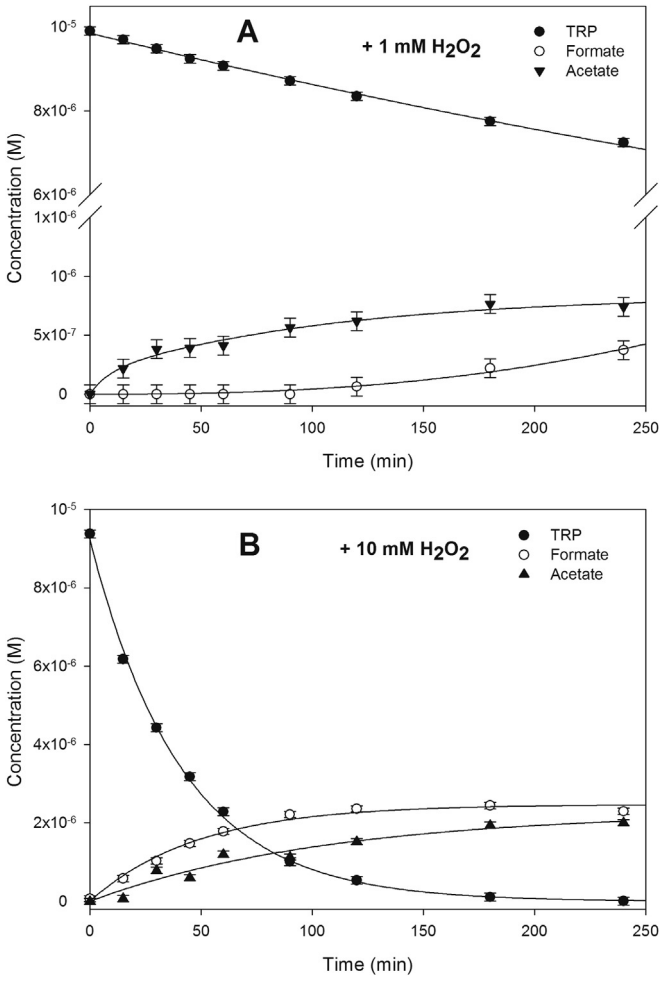

Fig. 5. Disappearance of TRP (10 μM) in the presence of H_2O_2 1 mM (**A**) and 10 mM (**B**) and the formation of formate and acetate under polychromatic irradiation in water at a pH of approximately 5.5 and T = 288 ± 3 K.

Hydrogen abstraction (pathway *iii*) can take place on the α-carbon, and the generated radical could be reduced to an unsaturated compound with a double bond between carbons in the α and β positions. The chemical structures of these compounds have been previously proposed (Domingues et al., 2003). The radical at the α-carbon could also undergo oxidative deamination (through imine) and produce a ketoacid ($[M+H]^+ = 204$ m/z) (Milne and Zika, 1993). The hydrogen abstraction could also take place at the β-carbon, leading to the formation of formic acid and a resonance-stabilized radical intermediate; this intermediate could lead to an imine by H-transfer. The imine can be easily hydrolysed in water to form an aldehyde detected by MS at $[M+H]^+ = 160$ m/z. The further oxidation of the aldehyde by a hydroxyl radical could lead to fragmentation of the carbon chain with the production of acetic acid and formation of indole detected by ion chromatography and mass spectrometry, respectively.

The formation of carboxylic acids by the photo-oxidation of amino acids has also been suggested by Milne and Zika (1993). Tryptophan can absorb UV-light, and therefore, it can undergo direct photolysis. We have shown that the photolysis process in the presence and absence of hydrogen peroxide leads to the formation of the same products but with a prevalence of hydroxylated products in the case of irradiation in the presence of hydrogen peroxide. In the absence of photogenerated hydroxyl radicals, TRP could undergo photoionization, as reported in the literature for TRP and other indole derivatives (Creed, 1984; Temussi et al., 2011), leading to a radical intermediate. The decarboxylation of this intermediate followed by H-transfer could produce the same imine produced in presence of HO• (Temussi et al., 2011). The radicals produced during TRP irradiation could lead to a radical chain reaction with the formation of oxidized products and small carboxylic acids, as observed with hydrogen peroxide.

High molecular weight products are also detected at $[M+H]^+ = 332$ m/z and 334 m/z, with the ion at 334 m/z most likely being an adduct of tryptophan with 3-methyl indole. The ion at $[M+H]^+ = 332$ m/z corresponds to the reduced form of this adduct with a double bond between the α and β carbons of the tryptophan molecule (Domingues et al., 2003). Moreover, the product with a mass of $[M+H]^+ = 409$ m/z can be attributed to the dimer of TRP.

3.4. Fluorescence spectra of irradiated solutions

Fig. 7 reports the EEM spectra of a 10 μM TRP solution before (Fig. 7A) and after 4 h of irradiation in the presence of 100 μM H_2O_2 (Fig. 7B). In the presence of H_2O_2 under irradiation, the intensity of the TRP signal decreases, while another signal appears at λ_{ex} 330 nm and λ_{em} 425 nm (see the difference between 7B and 7A in Fig. 7). This signal is classified by Coble (Coble, 1996) as the fluorescence signal of HUmic LIke Substances. Domingues et al. (2003) show for the first time that the oxidation of TRP leads to the

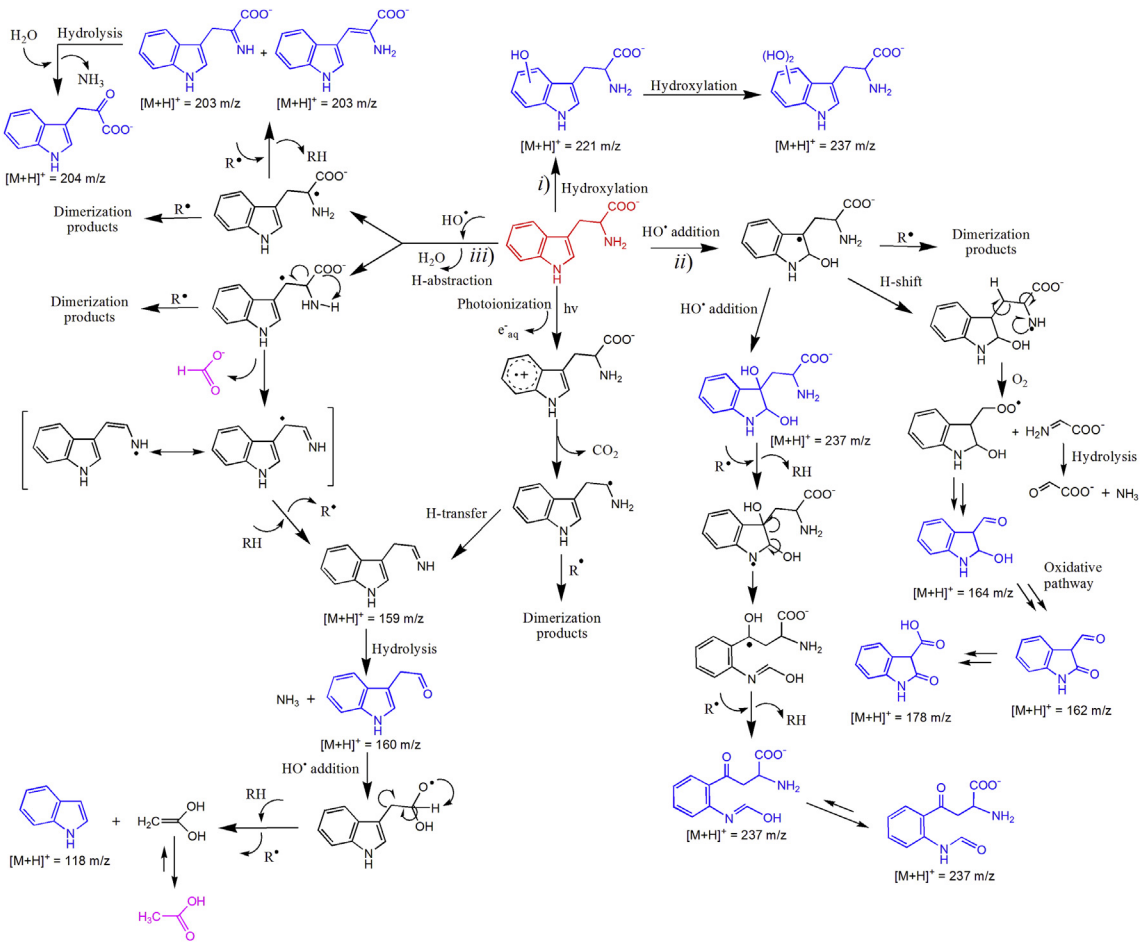

Fig. 6. Suggested transformation mechanism of TRP (red) in aqueous solution. In blue are the chemical structures proposed for products detected by MS-ESI, and in violet are the carboxylic acids detected by ion chromatography. (For interpretation of the references to colour in this figure legend, the reader is referred to the web version of this article.)

formation of compounds at higher molecular weights, as well as their hydroxylation products. The same fluorescent signal was previously reported under UV irradiation using a mM level of TRP in aqueous solution (Bianco et al., 2014). It could not be excluded that the fluorescence signal at $\lambda_{ex} = 330$ nm and $\lambda_{em} = 425$ nm is due to these species, for which the molecular weight and oxidation could be compared to the spectroscopic signature of HULIS or FULIS. Under direct photolysis (Figure SM3), no signal corresponding to HULIS formation is detected.

4. Atmospheric relevance and conclusions

TRP is found in cloud water from oceanic and continental origin, and its concentration is estimated to be on the order of 10^{-7} to 10^{-8} M. Considering the second order rate constant between TRP and HO• ($k_{HO^{\bullet},TRP}$) of 1.3×10^{10} M^{-1} s^{-1} (Buxton et al., 1998), we can compare the hydroxyl radical scavenging ability of TRP with those of other relevant short-chain carboxylic acids, such as acetic, oxalic and succinic acids, that are generally found in concentrations of a few micromolar in cloud water. This value can be correlated to the fraction of HO• scavenged by DOC (Dissolved Organic Matter), considering the $k_{HO^{\bullet},DOC}$ of 3.8×10^8 L molC^{-1} s^{-1} (Arakaki et al., 2013). The HO• inhibition ($I_{HO^{\bullet}}$, %) for TRP and selected carboxylic acids can be estimated for each cloud water sample using Eq. (3):

$$I_{HO^{\bullet}}\ (\%) = \frac{[A] \times k_{HO^{\bullet},A}}{[DOC] \times k_{HO^{\bullet},DOC}} \times 100 \qquad (3)$$

where [A] and $k_{HO^{\bullet},A}$ are the concentration and second order rate constant with HO• of the considered species *A*, and [DOC] $\times$ $k_{HO^{\bullet},DOC}$ is determined considering the DOC concentration of each sample (see Table SM2). In Fig. 8, the contributions are reported considering a pH of 6.0 and the relative concentrations of the acidic and basic forms of species thereafter (see SM). The contribution of TRP is between 0.07 and 0.38% for samples n° 1, 12, 15 and 16, while the concentrations for cloud water samples n° 4 and 8 rise up to 2.50 and 4.55%, respectively. Moreover, considering that TRP is only one of the essential amino acids, we can argue that investigating the concentrations of amino acids and their transformation is crucial to better assess the organic matter composition and hydroxyl radical reactivity in cloud water.

In this work, we demonstrated that TRP reactivity with hydroxyl radicals occurs following different reactivity pathways: *1*) formation of hydroxylated products, *2*) formation oligomeric compounds with similar fluorescence characteristics to those reported for HULIS, *3*) formation of decarboxylated compounds such as *N*-formylkynurenine and *4*) formation of short chain carboxylic acids. The phototransformation of TRP (direct and HO•-mediated) in cloud water can be considered to be a new source of short chain organic compounds and HULIS. These results highlight the importance of the complementary approach (*i.e.*, characterization and

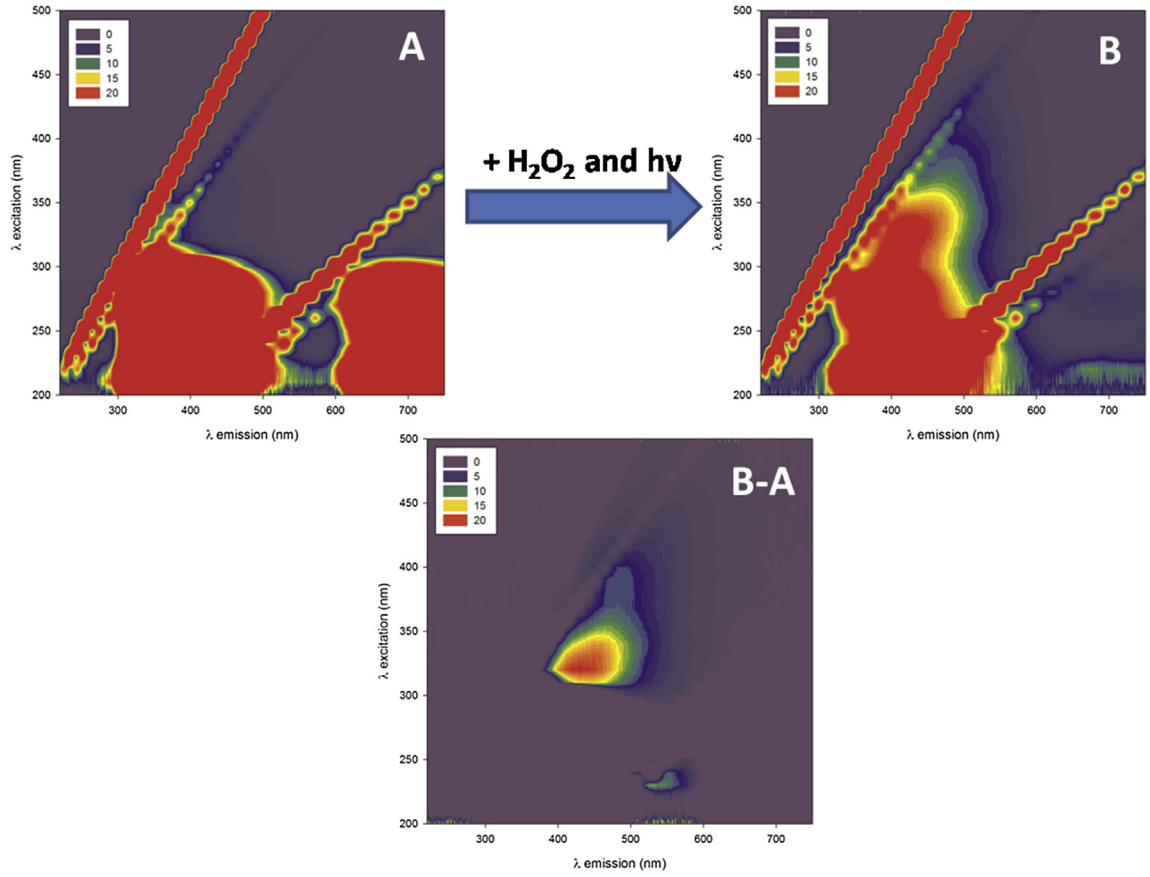

Fig. 7. EEM (as a contour plot) of 10 μM TRP (**A**) and an irradiated solution for 4 h in the presence of 100 μM H_2O_2 (**B**). The difference between the two EEM normalized for the TRP concentration is reported as **B-A**.

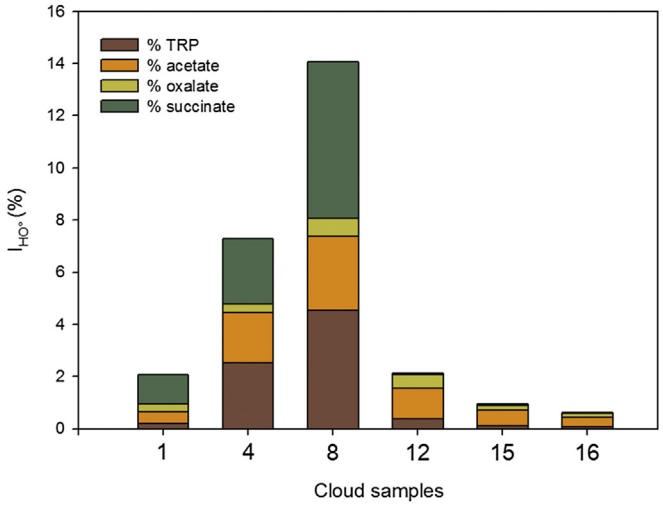

Fig. 8. HO• inhibition ($I_{HO^•}$, %) by TRP, acetate, oxalate and succinate. Values are estimated considering a pH of 6.0. The relative concentration of each species is reported in the SM.

reactivity assessment) in improving the understanding of photochemical and hydroxyl radical-driven transformations in this medium. Certainly, the real impact of proteinogenic amino acid transformation depends on their concentrations and on the oxidative properties of the cloud aqueous phase.

Acknowledgements

Authors acknowledge financial support from the Regional Council of Auvergne, from the "Fédération de Recherches en Environnement" through the CPER "Environnement" founded by the "Région Auvergne," the French government, FEDER from the European community, and program ANR BIOCAP (ANR-13-BS06-0004).

Appendix A. Supplementary data

Supplementary data related to this article can be found at http://dx.doi.org/10.1016/j.atmosenv.2016.04.034.

References

Arakaki, T., Anastasio, C., Kuroki, Y., Nakajima, H., Okada, K., Kotani, Y., Handa, D., Azechi, S., Kimura, T., Tsuhako, A., Miyagi, Y., 2013. A general scavenging rate constant for reaction of hydroxyl radical with organic carbon in atmospheric waters. Environ. Sci. Technol. 47, 8196–8203.

Barbaro, E., Zangrando, R., Vecchiato, M., Piazza, R., Cairns, W.R.L., Capodaglio, G., Barbante, C., Gambaro, A., 2015. Free amino acids in Antarctic aerosol: potential markers for the evolution and fate of marine aerosol. Atmos. Chem. Phys. 15, 5457–5469.

Bianco, A., Minella, M., De Laurentiis, E., Maurino, V., Minero, C., Vione, D., 2014. Photochemical generation of photoactive compounds with fulvic-like and humic-like fluorescence in aqueous solution. Chemosphere 111, 529–536.

Bianco, A., Passananti, M., Perroux, H., Voyard, G., Mouchel-Vallon, C., Chaumerliac, N., Mailhot, G., Deguillaume, L., Brigante, M., 2015. A better understanding of hydroxyl radical photochemical sources in cloud waters collected at the puy de Dôme station: experimental vs. modeled formation rates. Atmos. Chem. Phys. 15, 13923–13955.

Buxton, G.V., Greenstock, C.L., Helman, W.P., Ross, A.B., 1998. Critical review of rate

constants for reactions of hydrated electrons, hydrogen atoms and hydroxyl radicals ($^{\bullet}OH/^{\bullet}O^{-}$) in aqueous solution. J. Phys. Chem. Ref. Data 17, 513–886.
Chan, M.N., Choi, M.Y., Ng, N.L., Chan, C.K., 2005. Hygroscopicity of water-soluble organic compounds in atmospheric aerosols: amino acids and biomass burning derived organic species. Environ. Sci. Technol. 39, 1555–1562.
Coble, P.G., 1996. Characterization of marine and terrestrial DOM in seawater using excitation-emission matrix spectroscopy. Mar. Chem. 51, 325–346.
Creed, D., 1984. The photophysics and photochemistry of the near-UV absorbing amino acids l-tryptophan and its simple derivative. Photochem. Photobiol. 39, 537–562.
De Haan, D.O., Corrigan, A.L., Tolbert, M.A., Jimenez, J.L., Wood, S.E., Turley, J.J., 2009. Secondary organic aerosol formation by self-reactions of methylglyoxal and glyoxal in evaporating droplets. Environ. Sci. Technol. 43, 8184–8190.
Deguillaume, L., Charbouillot, T., Joly, M., Vaitilingom, M., Parazols, M., Marinoni, A., Amato, P., Delort, A.M., Vinatier, V., Flossmann, A., Chaumerliac, N., Pichon, J.M., Houdier, S., Laj, P., Sellegri, K., Colomb, A., Brigante, M., Mailhot, G., 2014. Classification of clouds sampled at the puy de Dôme (France) based on 10 yr of monitoring of their physicochemical properties. Atmos. Chem. Phys. 14, 1485–1506.
Deguillaume, L., Leriche, M., Amato, P., Ariya, P.A., Delort, A.M., Poschl, U., Chaumerliac, N., Bauer, H., Flossmann, A.I., Morris, C.E., 2008. Microbiology and atmospheric processes: chemical interactions of primary biological aerosols. Biogeosciences 5, 1073–1084.
Després, V.R., Huffman, J.A., Burrows, S.M., Hoose, C., Safatov, A.S., Buryak, G., Frohlich-Nowoisky, J., Elbert, W., Andreae, M.O., Poschl, U., Jaenicke, R., 2012. Primary biological aerosol particles in the atmosphere: a review. Tellus B 64, 15598.
Determann, S., Lobbes, J.M., Reuter, R., Rullkotter, J., 1998. Ultraviolet fluorescence excitation and emission spectroscopy of marine algae and bacteria. Mar. Chem. 62, 137–156.
Domingues, M.R.M., Domingues, P., Reis, A., Fonseca, C., Amado, F.M.L., Ferrer-Correia, A.J.V., 2003. Identification of oxidation products and free radicals of tryptophan by mass spectrometry. J. Am. Soc. Mass Spectrom. 14, 406–416.
Dulin, D., Mill, T., 1982. Development and evaluation of sunlight actinometers. Environ. Sci. Technol. 16, 815–820.
Ge, X., Wexler, A.S., Clegg, S.L., 2011. Atmospheric amines - part I. A review. Atmos. Environ. 45, 524–546.
Herckes, P., Valsaraj, K.T., Collett Jr., J.L., 2013. A review of observations of organic matter in fogs and clouds: origin, processing and fate. Atmos. Res. 132–133, 434–449.
Herrmann, H., Schaefer, T., Tilgner, A., Styler, S.A., Weller, C., Teich, M., Otto, T., 2015. Tropospheric aqueous-phase chemistry: kinetics, mechanisms, and its coupling to a changing gas phase. Chem. Rev. 115, 4259–4334.
Hinman, R.L., Lang, J., 1965. Peroxidase-catalyzed oxidation of indole-3-acetic acid. Biochemistry 4, 144–158.
Hock, N., Schneider, J., Borrmann, S., Rompp, A., Moortgat, G., Franze, T., Schauer, C., Poschl, U., Plass-Dulmer, C., Berresheim, H., 2008. Rural continental aerosol properties and processes observed during the Hohenpeissenberg Aerosol Characterization Experiment (HAZE2002). Atmos. Chem. Phys. 8, 603–623.
Hudson, N., Baker, A., Reynolds, D., 2007. Fluorescence analysis of dissolved organic matter in natural, waste and polluted waters—a review. River Res. Appl. 23, 631–649.
Kuznetsova, M., Lee, C., Aller, J., 2005. Characterization of the proteinaceous matter in marine aerosols. Mar. Chem. 96, 359–377.
Mace, K.A., Artaxo, P., Duce, R.A.C., 2003a. Water-soluble organic nitrogen in Amazon Basin aerosols during the dry (biomass burning) and wet seasons. J. Geo. Res. Atmos. 108.
Mace, K.A., Kubilay, N., Duce, R.A.C., 2003b. Organic nitrogen in rain and aerosol in the eastern Mediterranean atmosphere: an association with atmospheric dust. J. Geo. Res. Atmos. 108.
Mandalakis, M., Apostolaki, M., Tziaras, T., Polymenakou, P., Stephanou, E.G., 2011. Free and combined amino acids in marine background atmospheric aerosols over the Eastern Mediterranean. Atmos. Environ. 45, 1003–1009.
Matsumoto, K., Uematsu, M., 2005. Free amino acids in marine aerosols over the western North Pacific Ocean. Atmos. Environ. 39, 2163–2170.
Mayer, L.M., Schick, L.L., Loder Iii, T.C., 1999. Dissolved protein fluorescence in two Maine estuaries. Mar. Chem. 64, 171–179.
McFiggans, G., Artaxo, P., Baltensperger, U., Coe, H., Facchini, M.C., Feingold, G., Fuzzi, S., Gysel, M., Laaksonen, A., Lohmann, U., Mentel, T.F., Murphy, D.M., O'Dowd, C.D., Snider, J.R., Weingartner, E., 2006. The effect of physical and chemical aerosol properties on warm cloud droplet activation. Atmos. Chem. Phys. 6, 2593–2649.
McGregor, K.G., Anastasio, C., 2001. Chemistry of fog waters in California's Central Valley: 2. Photochemical transformations of amino acids and alkyl amines. Atmos. Environ. 35, 1091–1104.
Milne, P., Zika, R., 1993. Amino acid nitrogen in atmospheric aerosols: occurrence, sources and photochemical modification. J. Atmos. Chem. 16, 361–398.
Mochizuki, T., Kawamura, K., Aoki, K., 2015. Water-soluble organic nitrogen in high mountain snow samples from central Japan. Aerosol Air Qual. Res. http://dx.doi.org/10.4209/aaqr.2015.04.025.
Möhler, O., DeMott, P.J., Vali, G., Levin, Z., 2007. Microbiology and atmospheric processes: the role of biological particles in cloud physics. Biogeosciences 4, 1059–1071.
Morris, C.E., Conen, F., Alex Huffman, J., Phillips, V., Pöschl, U., Sands, D.C., 2014. Bioprecipitation: a feedback cycle linking earth history, ecosystem dynamics and land use through biological ice nucleators in the atmosphere. Glob. Change Biol. 20, 341–351.
Muller, C.L., Baker, A., Hutchinson, R., Fairchild, I.J., Kidd, C., 2008. Analysis of rainwater dissolved organic carbon compounds using fluorescence spectrophotometry. Atmos. Environ. 42, 8036–8045.
Scalabrin, E., Zangrando, R., Barbaro, E., Kehrwald, N.M., Gabrieli, J., Barbante, C., Gambaro, A., 2012. Amino acids in Arctic aerosols. Atmos. Chem. Phys. 12, 10453–10463.
Scheller, E., 2001. Amino acids in dew - origin and seasonal variation. Atmos. Environ. 35, 2179–2192.
Schwier, A.N., Viglione, G.A., Li, Z., Faye McNeill, V., 2013. Modeling the surface tension of complex, reactive organic-inorganic mixtures. Atmos. Chem. Phys. 13, 10721–10732.
Spracklen, D.V., Heald, C.L., 2014. The contribution of fungal spores and bacteria to regional and global aerosol number and ice nucleation immersion freezing rates. Atmos. Chem. Phys. 14, 9051–9059.
Suzuki, J., Ueki, T., Shimizu, S., Uesugi, K., Suzuki, S., 1985. Formation of mutagens by photolysis of amino acids in neutral aqueous solution containing nitrite or nitrate ion. Chemosphere 14, 493–500.
Temussi, F., Cermola, F., DellaGreca, M., Iesce, M.R., Passananti, M., Previtera, L., Zarrelli, A., 2011. Determination of photostability and photodegradation products of indomethacin in aqueous media. J. Pharm. Biomed. Anal. 56, 678–683.
Turjanski, A.G., Rosenstein, R.E., Estrin, D.A., 1998. Reactions of melatonin and related indoles with free radicals: a computational study. J. Med. Chem. 41, 3684–3689.
Vivian, J.T., Callis, P.R., 2001. Mechanisms of tryptophan fluorescence shifts in proteins. Biophys. J. 80, 2093–2109.
Wedyan, M.A., Preston, M.R., 2008. The coupling of surface seawater organic nitrogen and the marine aerosol as inferred from enantiomer-specific amino acid analysis. Atmos. Environ. 42, 8698–8705.
Zhang, Q., Anastasio, C., 2001. Chemistry of fog waters in California's Central Valley—Part 3: concentrations and speciation of organic and inorganic nitrogen. Atmos. Environ. 35, 5629–5643.
Zhang, Q., Anastasio, C., 2003. Free and combined amino compounds in atmospheric fine particles (PM2.5) and fog waters from Northern California. Atmos. Environ. 37, 2247–2258.
Zhang, Q., Anastasio, C., Jimenez-Cruz, M., 2002. Water-soluble organic nitrogen in atmospheric fine particles (PM2.5) from northern California. J. Geo. Res. Atmos. 107. AAC 3-1-AAC 3–9.
Zhu, C., Kawamura, K., Kunwar, B.C.J.D., 2015. Organic tracers of primary biological aerosol particles at subtropical Okinawa Island in the western North Pacific Rim. J. Geo. Res. Atmos. 120, 5504–5523.